Sharp-Line Electronic Spectroscopy and Ligand Field Analysis of *cis*-(1,4,8,11-Tetraazacyclotetradecane)-(ethylenediamine)chromium(III)[1]

Jong-Ha Choi* and In-Gyung Oh

Department of Chemistry, Andong National University, Andong 760-749
Received October 19, 1992

The 77 K luminescence and excitation, room-temperature visible spectra of *cis*-[Cr(cyclam)(en)]$(ClO_4)_3$ (cyclam=1,4,8,11-tetraazacyclotetradecane, en=ethylenediamine) have been measured. It is found that the zero-phonon line in the excitation spectrum splits into two components by 40 cm^{-1}. The eight pure electronic bands due to spin-allowed and spin-forbidden transitions are assigned. Ligand field parameter set for the complex has been determined from broad band and sharp-line electronic spectra by means of modern ligand field theory based on the angular overlap model. As expected, the results of the optimization indicate that the nitrogen atoms of en and cyclam have a strong σ-donor property toward chromium(III).

Introduction

In the past two decades a considerable amount of data from the sharp-line electronic spectroscopy has been accumulated, although the some assignments are still tentative and controversial.[2] It has been recognized that the sharp-line electronic transitions may be useful to extract geometric informations.[3] The transitions to the ^2E_g and $^2T_{1g}$ states in octahedral chromium(III) complexes give rise to very sharp lines because the slopes of the energy lines for the these states are same as that for the ground state except in extremely weak field.[4] In contrast to broad band (interconfigurational) spectra, sharp-line (intraconfigurational) transitions of metal complexes are quite sensitive to the bond angles around the metal. Therefore, it is possible to obtain a structural information from the sharp-line electronic spectroscopy without a full X-ray structure determination.

It has been suggested that macrocyclic complexes of transition metals have similar properties to biologically important systems. Cyclam structures resemble porphyrins in that both systems are cyclic tetradentate nitrogen donor ligands.[5] In addition to, ruthenium(II) and chromium(III) complexes have been used for experiments in photochemical energy storage because their lowest energy excited states are long-lived and capable of a rapid electron-transfer reaction.[6] In CrN_6 type complexes the spectral features are very similar. However, we expect that the photochemical quantum yields vary considerably.[7]

In this paper we report a study on the 77 K luminescence and excitation, and room-temperature absorption spectra of *cis*-[Cr(cyclam)(en)]$(ClO_4)_3$ including the assignments of the observed bands. The complex is of interest because it displays the five sharp electronic lines in the excitation spectrum. The results of modern ligand field analysis of the observed electronic bands are also discussed.

Experimental

Synthesis. The free ligand cyclam was purchased from Strem Chemicals. All other materials were of reagent grade and used without further purification. *cis*-[Cr(cyclam)(en)]$(ClO_4)_3$ was prepared according to the literature procedure.[8] The compound was recrystallized three times for spectroscopic measurements.

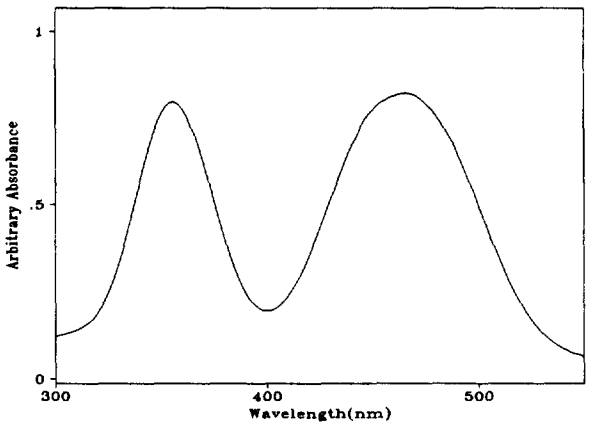

Figure 1. Electronic absorption spectrum of *cis*-$[Cr(cyclam)(en)]^{3+}$ in aqueous solution at room-temperature.

Spectroscopic Measurements. Room-temperature absorption spectrum of freshly prepared aqueous solution was recorded with a HP 8452 spectrophotometer. Luminescence and excitation spectra were recorded at 77 K on a Spex Fluorolog-2 spectrofluorometer. For measurements at 77 K the microcrystalline sample was placed in a quartz tube of 4 mm i.d. and directly immersed in a Dewar flask which had a quartz tail and was filled with liquid nitrogen as previously described.[9] The wavelength scale of the spectrofluorometer was calibrated with the lines from a low-pressure mercury lamp.

Results and Discussion

Absorption Spectrum. The visible absorption spectrum of *cis*-[Cr(cyclam)(en)]$(ClO_4)_3$ in aqueous solution is represented in Figure 1. It exhibits two ligand field absorption bands, one at 465.30 nm (21490 cm^{-1}, ν_1) and the other at 356.16 nm (28077 cm^{-1}, ν_2) corresponding to the $^4A_{2g}\rightarrow{}^4T_{2g}$ and $^4A_{2g}\rightarrow{}^4T_{1g}$ (O_h) transitions, consistent with quasioctahe-

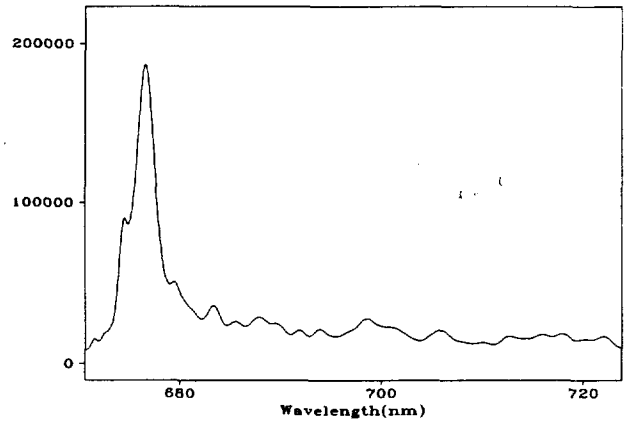

Figure 2. Luminescence spectrum of *cis*-[Cr(cyclam)(en)]$(ClO_4)_3$ at 77 K.

dral coordination of six amine ligands.

Within a conventional ligand field theory, the energy of the first spin-allowed transition, $^4A_{2g}\rightarrow{}^4T_{2g}$ (ν_1) directly gives the value of ligand field parameter, $10Dq$. It is shown that the value of ratio, ν_2/ν_1 is 1.307. We can find that this value corresponds with $Dq/B=3.481$, $\nu_3/B=74.327$, $\nu_3/\nu_1=2.124$ and $\nu_3/\nu_2=1.626$ from the table[10] of transition energy ratios for octahedral chromium(III) complexes. The angular overlap model parameter, e_σ is readily obtained from the relation, $10Dq=3e_\sigma-4e_\pi$ because the π-bonding for the amine nitrogen is zero approximately.[10] However, it is noteworthy that the π-bonding ability of nitrogen with sp^2 hybridization such as peptide nitrogen is a weak π-donor.[9] The deduced ligand parameters based on the broad band spectrum for *cis*-[Cr(cyclam)(en)]$^{3+}$ are $Dq=2149$, $B=615$ and $e_\sigma(N)=7163$ cm^{-1}. These parameters can be used as an input data for complete ligand field analysis including the sharp-line electronic transitions. The position of transition to the $^4T_{1g}$(P) state is also predicted to lie at about 219.0 nm (45644 cm^{-1}, ν_3) from the energy ratio. The third band corresponding to this transition has not been observed because it is masked by intense liqand or charge-transfer absorption in the uv-visible spectrum.

Luminescence Spectrum. The 466 nm excited luminescence spectrum of *cis*-[Cr(cyclam)(en)]$(ClO_4)_3$ at 77 K is shown in Figure 2. The peak positions and vibronic intervals are also given in Table 1.

The strongest narrow peak at 14782 cm^{-1} (676.5 nm) in the luminescence spectrum, which is assigned to the zero-phonon line, R_1 because corresponding the strong peak is found at 14797 cm^{-1} (675.8 nm) in the excitation spectrum. A hot band appeared at 14828 cm^{-1} (674.4 nm) may be assigned to the second component of the $^2E_g\rightarrow{}^4A_{2g}$ transition. The splitting of zero-phonon line in the luminescence spectrum was obtained by deconvolution to be 46 cm^{-1}. The vibronic intervals occurring in the spectrum consist of several modes presumed to involve primary ring torsion and angle bending with frequencies below 369 cm^{-1}. The N-Cr-N bending modes can be assigned to the 243 and 277 cm^{-1} vibronic peaks, similar to values[11] reported for δ(N-Cr-N) in $[Cr(NH_3)_6]^{3+}$. The Cr-N stretching modes are found at 435 and 468 cm^{-1} in the spectrum. A medium absorption peak at 614 cm^{-1} is due to ionic perchlorate.[12] The weak

Table 1. Luminescence Data for *cis*-[Cr(cyclam)(en)]$(ClO_4)_3$[a]

λ/nm	$\bar{\nu}$/cm^{-1}	$\bar{\nu}_0-\bar{\nu}$/cm^{-1}	Assignment
671.5	14892	−110 vw	
674.4	14828	−46 s	R_2
676.5	14782	0 vs	R_1
679.4	14719	63 w	
683.4	14630	149 m	Lattice mode
685.5	14588	194 w	
687.8	14539	243 m	δ(N-Cr-N)
689.4	14505	277 vw	
691.8	14455	327 w	
693.8	14413	369 w	
697.0	14347	435 sh	ν(Cr-N)
698.6	14314	468 m	
701.3	14259	523 sh	ν(Cr-N) + Ring def.
705.8	14168	614 m	ClO_4^-
710.0	14085	697 vw	
712.7	14031	751 w	ρ(CH_2)
715.9	13968	814 w	
717.9	13930	852 w	ρ(NH_2)
720.2	13885	897 vw	
722.0	13850	932 w	γ(NH_2)

[a]Data in cm^{-1}.

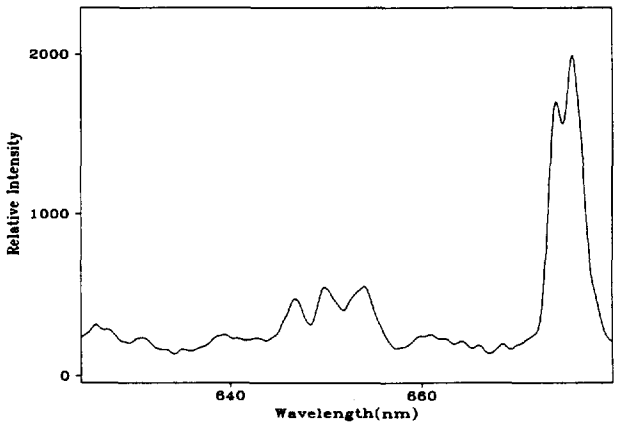

Figure 3a. Excitation spectrum of *cis*-[Cr(cyclam)(en)]$(ClO_4)_3$ at 77 K.

bands in the 750-852 cm^{-1} region are primarily involved in the NH_2 and CH_2 rocking modes.[13] The spectrum did not change with the exciting wavelength within the first spin-allowed bands.

Excitation Spectrum. The 77 K excitation spectrum is shown in Figure 3a and peak positions with their assignments are tabulated in Table 2. The spectrum was obtained by monitoring the luminescence intensity of the vibronic sideband at 698 nm. The mirror image relationship between the luminescence and excitation spectrum is quite apparent on comparison of the two spectra. Figure 3b also shows the portion of $^4A_{2g}\rightarrow{}^2T_{1g}$ electronic origin (T_1, T_3 and T_3) on an expanded scale and their Gaussian resolved components. Two strong peaks at 14797 cm^{-1} (675.8 nm) and 14837 cm^{-1} (674.0 nm) coincide with peaks in the luminescence spectrum and are assigned to the two components of the lowest energy

Table 2. Peak Positions in the 77 K Sharp-Line Excitation Spectrum of *cis*-[Cr(cyclam)(en)](ClO$_4$)$_3$[a]

$\bar{\nu}$−14797	Assignment	(Calcd)[b]	Vibronic frequencies		Ground state frequencies[c]
0 vs	R_1		ν_1	162	149
40 vs	R_2		ν_2	253	243
160 w	$R_1+\nu_1$	(162)	ν_3	355	369
218 w	$R_2+\nu_1$	(202)	ν_4	467	468
259 vw	$R_1+\nu_2$	(253)			
300 w	$R_2+\nu_2$	(293)			
332 w	$R_1+2\nu_1$	(324)			
357 vw	$R_1+\nu_3$	(355)			
492 s	T_1				
523 w	$R_1+\nu_1+\nu_3$	(517)			
565 m	$R_2+\nu_1+\nu_3$	(557)			
595 s	T_2				
663 s	T_3				
696 vw					
760 vw	$T_2+\nu_1$	(757)			
808 vw	$T_1+2\nu_1$	(816)			
843 w	$T_2+\nu_2$	(848)			
909 vw	$T_3+\nu_2$	(916)			
951 w	$T_1+\nu_4$	(959)			
996 sh	$T_3+2\nu_1$	(987)			
1053 w	$T_2+\nu_4$	(1062)			
1147 sh	$T_3+\nu_4$	(1130)			
1177 w	$T_3+\nu_1+\nu_3$	(1181)			

[a] Data in cm^{-1}. [b] Values in parentheses represent the calculated frequency of the vibrational mode listed. [c] From the luminescence spectrum (Table 1).

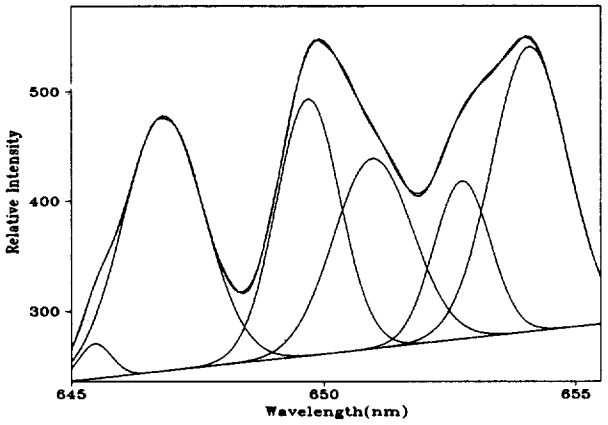

Figure 3b. Expanded portion of the $^4A_{2g}\rightarrow{}^2T_{1g}$ electronic origins and their resolved Gaussian components in the excitation spectrum.

electronic $^4A_{2g}\rightarrow{}^2E_g$ transition. The position of the R_1 line was 15 cm^{-1} lower than the same line observed in the luminescence spectrum. The apparent discrepancy is traceable to the experimental uncertainties from the procedure of calibration. The zero-phonon band splitting of observed 40 cm^{-1} may be compared with the 18 cm^{-1} for [Cr(en)$_3$]Cl$_3$, 10 cm^{-1} for [Cr(tacn)$_2$]Cl$_3$ (tacn=1,4,7-triazacyclononane), and 50 cm^{-1}

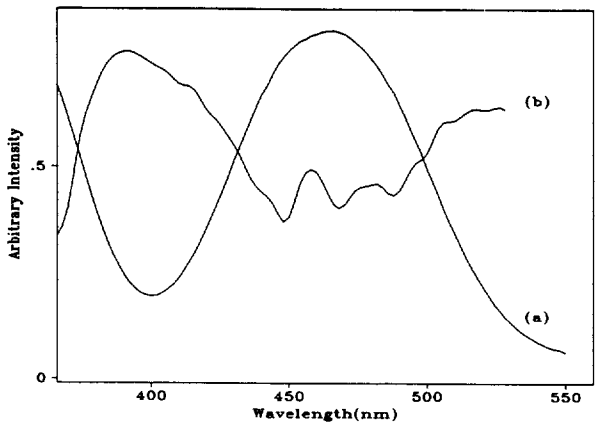

Figure 4. Absorption spectrum(labeled with a) and second derivative spectrum(labeled with b) of *cis*-[Cr(cyclam)(en)]$^{3+}$ in aqueous solution.

Table 3. Optimized Cartesian and Spherical Polar Coordinates for Ligating Nitrogen Atoms in *cis*-[Cr(cyclam)(en)](ClO$_4$)$_3$[a]

Atom	x	y	z	θ	φ
N_1	−0.1136	−2.0702	0.0901	87.51	−93.14
N_2	0.1473	−0.0788	−2.0852	175.42	−28.15
N_3	−2.0767	0.1619	−0.0905	90.55	175.54
N_4	0.0783	−0.1481	2.0851	92.53	3.56
N_5	−0.1499	2.0776	0.0202	4.59	−62.14
N_6	0.1121	0.0051	1.9846	89.44	94.13

[a] Coordinates are in Å.

for *cis*-[Cr(cyclam)(pn)](ClO$_4$)$_3$, respectively.[14-16]

The three components of the $^4A_{2g}\rightarrow{}^2T_{1g}$ electronic origin are found with strong intensities at 492, 595 and 663 cm^{-1} from the lowest electronic line, R_1. An experimental problem lies with the difficulty in distinguishing pure electronic peaks from the vibronic bands also appear in the spectrum. In general, it is known that the electronic lines are more intense than the vibronic peaks in the same area. We can find that the five electronic transition peaks stand out well and demonstrate a typical 2-3 splitting pattern in the excitation spectrum of Figure 3a.

The higher energy $^4A_{2g}\rightarrow{}^2T_{21g}$ band was found at 22321 cm^{-1} (448.0 nm) from the second derivative of the solution absorptions spectrum of *cis*-[Cr(cyclam)(en)]$^{3+}$ as shown with labeled (b) in Figure 4, but could not be resolved into the separate components.

Ligand Field Analysis. The ligand field potential was constructed with only the six coordinated nitrogen atoms. The nitrogen angular positions to generate the geometric factors for the ligand field potential were taken from the known X-ray crystal structure.[17] We also optimized the alignment of the coordinated nitrogen atoms with Cartesian axes centered on the chromium ion. The resulting Cartesian and spherical polar coordinates for the ligating atoms are listed in Table 3. The angular overlap parameter provides more chemical insight and will be used to interpret of the electronic spectrum.

Hoggard[3] has described the general method to determine

Table 4. Experimental Electronic and Calculated Transition Energies for *cis*-[Cr(cyclam)(en)]$(ClO_4)_3$[a]

State(O_h)	Exptl	Calcd[b]
^2E_g	14797	14808
	14837	14820
$^2T_{1g}$	15289	15314
	15392	15390
	15460	15439
$^2T_{2g}$ (avg)	22321	22356
$^4T_{2g}$ (avg)	21490	21410
$^4T_{1g}$ (avg)	28077	28112

[a] All data in cm^{-1}, [b] $e_{\sigma N}=7357(9)$, $B=679(2)$, $C=3045(6)$, $\alpha_T=82(3)$, $\zeta=275(24)$.

the eigenvalues and eigenfunctions of a d^3 configuration in a ligand field from any number of atoms in any geometry. The sharp-line transition energies, the eight components of the $^4A_{2g}\rightarrow{}^2E_g$, $^2T_{1g}$, and $^2T_{2g}$ transitions, are particulary sensitive to the geometry of the ligands and any other atoms perturbing the metal ion *d* orbitals. The full set of 120 single-term antisymmetrized product wavefunctions was used as a basis. The Hamiltonian function used in the calculation was

$$H=\sum_{i<j}\frac{e^2}{r_{ij}}+V_{LF}+\xi\sum_i l_i\cdot s_i+\alpha_T\sum_i l_i^2+2\alpha_T\sum_{i<j} l_i\cdot l_j \qquad (1)$$

the terms of which represent the interelectronic repulsion, the ligand field potential, the spin-orbit coupling, and the last two the Trees correction, respectively. The π-interaction of nitrogen with sp^3 hybridization were assumed to be negligible.[10]

Diagonalization of the 120×120 secular matrix yields the doublet and quartet energies with the appropriate degeneracies. The ligand field analysis was carried out through an optimized fit of experimental to calculated transition energies. The parameters varied during the optimization were the interelectronic repulsion parameters *B*, *C* and the Trees correction parameter α_T, the spin-orbit coupling parameter ζ and the AOM parameter $e_{\sigma N}$. These five parameters were used to fit eight experimental transition energies: the five $^4A_{2g}\rightarrow\{^2E_{2g}, {}^2T_{1g}\}$ components, identified in Table 4 and the average energies of the transitions to the $^2T_{2g}$, $^4T_{2g}$, and $^4T_{1g}$ states. Now it is possible to determine all ligand field parameters without the necessity of choosing one arbitrary. Eigenvalues were assigned to states within the doublet and quartet manifolds based on an analysis of the corresponding eigenfunctions.[18] The function minimized was

$$f=1000\,S^2+100\sum D^2+10\,T^2+\sum Q^2 \qquad (2)$$

where *S* in the first term is the ^2E_g splitting and *D*, *T*, and *Q* represent the differences between experimental and calculated $\{^2E_g, {}^2T_{1g}\}$, $^2T_{2g}$, and $\{^4T_{2g}, {}^4T_{1g}\}$ transition energies, respectively. The quartet terms were given a quite low weight factor to reflect the very large uncertainty in their positions. The Powell parallel subspace optimization procedure[19] was used to find the global minimum. The optimization was repeated several times with different sets of starting parameters to verify that the same global minimum was found. The results of the optimization and ligand field parameter set used to generate the best-fit energies are listed in Table 4.

The error margins reported for the best-fit parameters in Table 4 are those resulting from the propagation of experimental errors[20] of 30 cm^{-1} for the quartet positions, 10 cm^{-1} for the average $^2T_{2g}$ position, 3 cm^{-1} for each $\{^2E_g, {}^2T_{1g}\}$ peak, and 1 cm^{-1} for the ^2E_g splitting.

The value of 7357 cm^{-1} for $e_{\sigma N}$ parameter obtained from the complete ligand field theory is a little smaller than the 7608 cm^{-1} reported for $[Cr(tacn)_2]Cl_3$.[15] However, it is safe to conclude that nitrogen atoms of en and cyclam ligands have a strong σ-donor property. The value $e_{\sigma N}$ of characterizing the nitrogen atom is located in the normal range for ligating property toward chromium(III).[21] The parameters representing interelectronic repulsion and spin-orbit coupling terms may be compared with those of $[Cr(en)_3]Cl_3$ and $[Cr(tacn)_2]Cl_3$, respectively.[3b,15] There is a reduction in the Racah parameter *B* of the complex to about 74% of the free ion value. It is also found that the ratio of interelectronic parameters, *C*/*B*, is 4.485. The complete parameter set of ligand field reported here may be transferable to other complexes as a basis for schematic analysis of this type hexaamine system.

Acknowledgements. We wish to thank Professor P. E. Hoggard for his generous hospitality during our stay at NDSU. The financial support of the Korea Science and Engineering Foundation is also gratefully acknowledged.

References

1. (a) This is part 12 of the series "Electronic Structure and Chemical Reactivity of Transition Metal Complexes"; (b) The preceding publication in this series is Ref. 16.
2. (a) W. N. Shepard and L. S. Forster, *Theoret. Chim. Acta,* **20**, 135 (1971); (b) C. D. Flint, *Coord. Chem. Rev.,* **14**, 47 (1974); (c) S. Decurtins, H. U. Güdel, and K. Neuenschwander, *Inorg. Chem.,* **16**, 796 (1977); (d) K. W. Lee and P. E. Hoggard, *Inorg. Chem.,* **27**, 907 (1988); (e) H. Risen, *Inorg. Chem.,* **27**, 4677 (1988).
3. (a) P. E. Hoggard, *Coord. Chem., Rev.,* **70**, 85 (1986); (b) P. E. Hoggard, *Inorg. Chem.,* **27**, 3476 (1988).
4. A. W. Adamson, *Pure Appl. Chem.,* **24**, 451 (1970).
5. (a) C. R. Sperati, *Ph.D. Thesis,* The Ohio State University, 1971; (b) J. J. Christensen, D. J. Eatough, and R. M. Izatt, *Chem. Rev.,* **74**, 351 (1974); (c) F. A. Cotton and J. Czuchajowska, *Polyhedron,* **9**, 2553 (1990).
6. (a) N. Sutin, *J. Photochem.,* **10**, 19 (1979); (b) D. G. Whitten, *Acc. Chem. Res.,* **13**, 83 (1980); (c) H. Gsponer *et al., Inorg. Chim. Acta,* **189**, 207 (1991).
7. F. Wasgestian and E. Gowin, *Inorg. Chim. Acta,* **120**, L17 (1986).
8. A. D. Kirk and D. Heyd, *Inorg. Chem.,* **30**, 2453 (1991).
9. J. H. Choi and P. E. Hoggard, *Polyhedron,* **11**, 2399 (1992).
10. A. B. P. Lever, *Inorganic Electronic Spectroscopy,* 2nd ed., Elsevier, Amsterdam, 1984.
11. R. Acevedo, G. Diaz, and C. D. Flint, *Spectrochim. Acta.,* **41A**, 1397 (1985).
12. K. Nakamoto, *Infrared and Raman Spectra of Inorganic and Coordination Compounds,* 4th ed., John Wiley & Sons,

New York, 1986.
13. H. H. Schmidtke and D. Garthoff, *Inorg. Chim. Acta*, **2**, 357 (1968).
14. C. D. Flint and A. P. Matthews, *J. Chem. Soc. Faraday Trans. II*, **72**, 579 (1976).
15. K. W. Lee and P. E. Hoggard, *Transition Met. Chem.*, **16**, 377 (1991).
16. J. H. Choi, *Bull. Korean Chem. Soc.*, **14**, 118 (1993).
17. (a) A. D. Kirk and H. U. Güdel, *Inorg. Chem.*, **31**, 4564 (1992); (b) A. D. Kirk and D. Heyd, to be published.
18. P. E. Hoggard, *Inorg. Chem.*, **30**, 4644 (1991).
19. (a) M. J. D. Powell, *Computer J.*, **7**, 155 (1964); (b) J. L. Kuester and J. H. Mize, *Optimization Techniques with Fortran*, McGraw-Hill, New York, 1973.
20. A. A. Clifford, *Multivariate Error Analysis*, Wiley-Halsted, New York, 1973.
21. A. B. P. Lever, *Coord. Chem. Rev.*, **43**, 63 (1982).

Analysis of Steric Repulsion Forces in Atomic Force Microscope with Polyethylene Oxide in Aqueous Media

Sang Il Jeon* and Jeseph D. Andrade†

Department of Chemistry, Kangnung National University, Kangnung 210-702
†Departments of Bioengineering and Materials Science, University of Utah, Salt Lake City, Utah 84112, U.S.A., *Received October 27, 1992*

We present a theoretical analysis for the use of long-range intermolecular steric repulsion forces for imaging by atomic force microscope (AFM). Polyethylene oxide (PEO) is assumed to be terminally attaching to a spherical AFM tip in aqueous media. Only two long-range intermolecular forces (van der Waals attraction and steric repulsion) are considered. All calculated forces are near 10^{-11} N, which should not produce deformation of the soft protein surface. Calculations are presented as a function of surface density and chain length of terminally attached PEO, and other variables. Longer chain length and maximal surface density of terminally attached PEO to a smaller sized spherical AFM tip (modified AFM system) is appropriate to obtain optimum images of proteins on the surface.

Introduction

The atomic force microscope (AFM) can be used to obtain atomic scale images of observable surfaces[1-3]. The imaging contrast originates from intermolecular forces between the tip and the surface. The sample need not be a conductor to be imaged. The surfaces to be imaged can also be in an aqueous environment[3,4], which enables one to realistically image biological systems and monitor biological processes in real time. Most AFM research is performed in an air media[1,2,5,6] using short-range intermolecular forces[7,8]. Long-range intermolecular forces can reduce the risk of damage of the soft protein surface. Long-range intermolecular forces that have been utilized with the AFM are van der Waals force[9] in air and van der Waals and electrostatic forces[10] in aqueous media.

Polymers attached on solid surfaces immersed in a liquid medium are protected against aggregation by steric stabilization[11,12]. There exist long-range steric repulsion forces between two surfaces bearing such adsorbed polymer layers. These repulsive forces often exceed the long-range van der Waals and electrostatic forces acting between the bare surfaces[9]. Polyethylene oxide (PEO) surfaces are becoming recognized as exhibiting strongly reduced protein adsorption[14-20]. The protein-resistant character of PEO is generally recognized as a steric stabilization effect. The origin of these repulsive forces is attributed to two components[21-23]: the osmotic and elastic components. The osmotic component arises from the local increase in chain segment concentration upon compression resulting in the development of an osmotic pressure. The elastic component arises from the chain segments that have a tendency to extend themselves upon compression.

PEO can be attached to AFM tips of different sizes. The attached PEO can vary in molecular weight (chain length) and in number of chains per unit surface area (surface density), the 2 major molecular factors in steric repulsion[19,20]. In this paper we present a qualitative theoretical analysis of the steric repulsion forces of PEO attached to a spherical AFM tip interacting with a soft protein sample surface as a function of the surface density and chain length of PEO with the variation of the sizes of tip and sample surface.

Modeling

The shape of the tip is pyramidal and terminates in a point; the apex of the pyramid is approximated as a sphere[24]. PEO is assumed to be a neutral homopolymer with linear and flexible chains terminally attached to a spherical AFM tip (Figure 1(a)). The surface is assumed to be a hypothetical cylindrical protein adsorbed on mica. Although there can be various cylindrical shapes on the surface, only one unique cylindrical surface is considered (Figures 1(a)). It has a shape of circle from a top view. The surface is treated as one circle because that the assumed cylindrical surface is positioned under the PEO attached AFM tip and we consider